

Influence of deep sea environment on the performance of a LiFePO_4 polymer battery^{*}

Chang-wen ZHENG^{1,2}, Shi-yao ZHOU^{1,2}, Zi-qiang CHEN^{†‡1,2},
 Yun-long GE^{1,2}, De-yang HUANG^{1,2}, Jian LIU¹, Qi YANG^{1,2}

¹Collaborative Innovation Center for Advanced Ship and Deep-Sea Exploration, Shanghai Jiao Tong University, Shanghai 200240, China

²National Engineering Laboratory for Naval Architecture, Shanghai Jiao Tong University, Shanghai 200240, China

[†]E-mail: chenziqiang@sjtu.edu.cn

Received Dec. 5, 2017; Revision accepted May 11, 2018; Crosschecked Sept. 21, 2018

Abstract: A lithium-ion polymer battery cell is an ideal energy source for underwater vehicles due to its high energy density and small volume. However, the performance of lithium-ion batteries in a 10000 m deep sea is still unknown and is of particular concern in the design of 10000 m autonomous remote vehicles (ARVs). In this paper, we explore how the external characterizing parameters of a LiFePO_4 polymer battery during discharge are affected by a high pressure of 100 MPa and low temperature of 3 °C for simulating the conditions experienced in a 10000 m deep sea environment. An unscented Kalman filter (UKF) algorithm is applied to estimate the state of charge (SoC) of a battery to investigate the influence of high hydrostatic pressure on SoC estimation due to changes in parameters. The results indicate that the LiFePO_4 polymer battery works under 100 MPa hydrostatic pressure, but its parameters change obviously and influence SoC estimation. SoC estimation accuracy was improved through compensating the functions of open circuit voltage (OCV) versus the state of charge (OCV-SoC) of the battery in a 100 MPa hydrostatic pressure and a low temperature environment.

Key words: Lithium polymer battery performance; Deep sea environment; State of charge (SoC) estimation; Autonomous remote vehicle (ARV)

<https://doi.org/10.1631/jzus.A1700660>

CLC number: TM912


1 Introduction

Lithium-ion batteries have become a widely used power source for autonomous underwater vehicles (AUVs), autonomous remote vehicle (ARVs), and underwater gliders (Wang et al., 2012; Liu et al., 2017). The power sources of sub-sea vehicles like AUVs and ARVs have experienced several generations of development: magnesium/dissolved oxygen

seawater semi-fuel cells (Hasvold et al., 2004), valve-regulated lead-acid (VRLA) batteries, nickel-cadmium (NiCd) batteries, and alkaline aluminium/hydrogen peroxide semi-fuel cells (Hasvold et al., 1999; Hasvold and Johansen, 2002). The aim of this study is to investigate the performance of a lithium polymer battery at 100 MPa hydrostatic pressure, for application to a 10000 m battery-powered ARV which will be developed in the near future. In general, batteries as power sources for underwater vehicles are configured into two different structures: (1) batteries enclosed in a pressurized vessel and working in a dry space at normal atmospheric pressure; (2) batteries working in a compensated vessel at ambient pressure and electrically insulated from the seawater.

[‡] Corresponding author

^{*} Project supported by the National Natural Science Foundation of China (No. 51677119)

 ORCID: Chang-wen ZHENG, <https://orcid.org/0000-0002-7158-5689>; Zi-qiang CHEN, <https://orcid.org/0000-0002-7490-6273>

© Zhejiang University and Springer-Verlag GmbH Germany, part of Springer Nature 2018

Up to now, batteries of the first type have been the most widely used for underwater vehicles. But the mass/displacement ratio of a pressurized hull increases with the diving depth (Stevenson and Graham, 2003). There is an increase in the mass and volume penalty in providing space at normal atmospheric pressure for the energy system in a 10 000 m underwater vehicle. Thus, a deep diving ARV will benefit hugely from the removal of pressurization and operating the batteries at ambient pressure (Griffiths et al., 2004).

However, whether a battery would be able to work under 100 MPa pressure is still unclear. Several studies have investigated the performance of batteries under high hydrostatic pressure. Hasvold et al. (2006) investigated lithium polymer battery cells from three different vendors (A, B, C). All the cells were charged at normal atmospheric pressure and discharged with 1/5 C at 30 MPa pressure and room temperature. The results showed that cells from vendor A generated gas internally and “ballooned”. Cells from vendors B and C survived in the test which indicated the lithium polymer battery could work in a pressure compensated vessel at 30 MPa pressure corresponding to a sea depth of 3000 m. By being submerged in oil, sealed inside a titanium box and discharged at the same pressure (30 MPa) as the ambient environment, the LiMn_2O_4 lithium polymer cell behaved normally during the test, but the capacity of the cell was reduced (Hasvold and Størkersen, 2001).

The investigations above prove only that lithium polymer cells can work at a pressure of 30 MPa, and the method they used to check whether the cells could survive and work at ambient pressure was simply to measure the variation in cell terminal voltage. Since the electrical performance of a lithium polymer battery at high hydrostatic pressure is critical for aspects of SoC estimation and fault diagnosis in battery management system, it is important to test lithium polymer batteries at higher hydrostatic pressures. Rutherford and Doerffel (2005) tested a Kokam lithium polymer battery cell at both 0.1 MPa and 60 MPa, and the effect of low temperature in deep sea was also considered. An equivalent circuit model (ECM) with several parameters is used to describe the external electrical performance of the battery, in which the open circuit voltage (OCV)-SoC relations both in charge and discharge at different temperatures

and pressures were compared at the same time. The parameters of the ECM were calculated using voltage-time data, and the results showed that the battery could work normally at 60 MPa and the parameters of the ECM were greatly affected by the low temperature.

This paper reports the electrical performance of a LiFePO_4 polymer battery cell at 100 MPa hydrostatic pressure and examines the issues of SoC estimation. A hybrid pulse power characterization (HPPC) test was used to extract the parameters of the ECM in three temperature-pressure circumstances: 20 °C/0.1 MPa, 20 °C/100 MPa, and 3 °C/0.1 MPa. A dynamic stress test (DST) is conducted to simulate the dynamic operating condition of an ARV in deep sea to provide real-time data for SoC estimation.

2 Battery modeling

To model the battery's external electrical performance and implement the unscented Kalman filter (UKF) algorithm in SoC estimation, a model is needed to characterize the battery's electrical properties. The most commonly used models are electrochemical models and ECMs (Zou et al., 2016). Due to the computational complexity of partial differential equations, electrochemical models are less often applied in real-time management or control oriented applications. We use the ECM in this study to model the battery's external electrical performance and implement the UKF algorithm in SoC estimation. The ECM comprised an OCV, an ohmic internal resistance R_0 , and two parallel resistor-capacitance (R-C) networks (Fig. 1a). The resistance R_1 and the capacitance C_1 were used to model the distribution of reactivity for capturing the local properties of the electrolyte. The charge transfer resistance R_2 and double-layer capacitance C_2 were used to represent the interfacial impedance of the cell (Sidhu et al., 2015).

The differential equations of the ECM are as follows:

$$\frac{dV_1}{dt} = -\frac{V_1}{R_1 C_1} + \frac{I}{C_1}, \quad (1)$$

$$\frac{dV_2}{dt} = -\frac{V_2}{R_2 C_2} + \frac{I}{C_2}, \quad (2)$$

$$V_t = V_{oc} - V_1 - V_2 - IR_0, \quad (3)$$

$$V_{oc} = g(\text{SoC}), \quad (4)$$

$$\text{SoC} = \text{SoC}_0 + \frac{1}{Q_0} \int_0^t I(\tau) d\tau, \quad (5)$$

where I is the current, V_1 and V_2 are the voltages across the networks of R_1 - C_1 and R_2 - C_2 , respectively, V_t is the terminal voltage, V_{oc} is the OCV which is a nonlinear function of SoC, and Q_0 is the rated capacity of the battery. In this study, the OCV-SoC fitting function at 20 °C/0.1 MPa is

$$g(\text{SoC}) = a + b\text{SoC} - c\text{SoC}^2 - \frac{d}{\text{SoC}} - e \ln(\text{SoC}) - f \ln(1.1 - \text{SoC}), \quad (6)$$

where $a=0.9112$, $b=4.142$, $c=2.042$, $d=0.1583$, $e=1.459$, and $f=0.2217$. The fitting curve of OCV-SoC is shown in Fig. 1b.

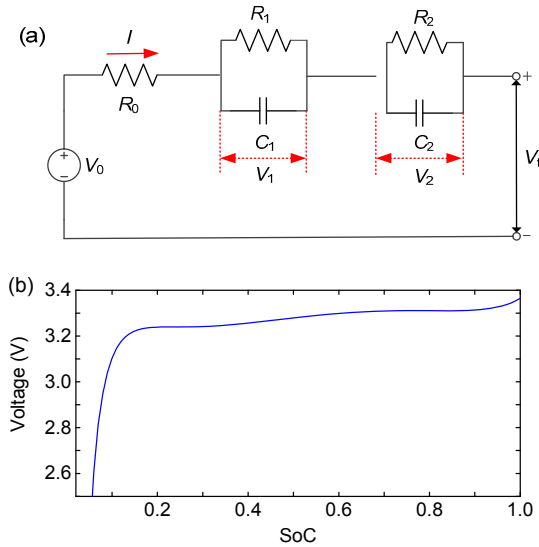


Fig. 1 A schematic of the second-order ECM (a); Fitting curve of OCV-SoC at 20 °C (b)

Considering a sampling time ΔT and time index k , Eqs. (1)–(5) can be transformed into discrete time format by using the zero-order hold method:

$$V_1(k+1) = e^{-\Delta T/(R_1 C_1)} V_1(k) + R_1 [1 - e^{-\Delta T/(R_1 C_1)}] I(k), \quad (7)$$

$$V_2(k+1) = e^{-\Delta T/(R_2 C_2)} V_2(k) + R_2 [1 - e^{-\Delta T/(R_2 C_2)}] I(k), \quad (8)$$

$$V_t(k) = g[\text{SoC}(k)] - V_1(k) - V_2(k) - R_0 I(k), \quad (9)$$

$$\text{SoC}(k+1) = \text{SoC}(k) + \frac{\Delta T I(k)}{Q_0}. \quad (10)$$

The cell is considered to be a nonlinear system with additive noise, as shown in Eqs. (11) and (12):

$$\mathbf{x}_{k+1} = f(\mathbf{x}_k, u_k) + \mathbf{w}_k, \quad (11)$$

$$y_k = h(\mathbf{x}_k, u_k) + v_k, \quad (12)$$

where \mathbf{x}_k is the state variable at time k , u_k is the input of the system at time k , y_k is the output of system at time k , the continuous nonlinear functions f and h are the state equation and measurement equation, respectively, \mathbf{w}_k is the process noise, and v_k is the measurement noise. Both \mathbf{w}_k and v_k are assumed to be mutually uncorrelated white Gaussian random processes with zero mean and variance:

$$E\{\mathbf{w}_k[l]\mathbf{w}_k^T[m]\} = \begin{cases} \mathbf{Q}, & l=m, \\ 0, & l \neq m, \end{cases} \quad (13)$$

$$E\{v_k[l]v_k^T[m]\} = \begin{cases} \mathbf{R}, & l=m, \\ 0, & l \neq m. \end{cases} \quad (14)$$

The state variable for the cell is $\mathbf{x}_k = [\text{SoC}(k), V_1(k), V_2(k)]^T$. Thus, the functions f and h can be transformed into discrete time format as Eqs. (15) and (16), respectively.

$$f(\mathbf{x}_k, u_k) = \begin{bmatrix} \text{SoC}(k) + \frac{\Delta T I(k)}{Q_0} \\ e^{-\frac{\Delta T}{R_1 C_1}} V_1(k) + R_1 [1 - e^{-\frac{\Delta T}{R_1 C_1}}] I(k) \\ e^{-\frac{\Delta T}{R_2 C_2}} V_2(k) + R_2 [1 - e^{-\frac{\Delta T}{R_2 C_2}}] I(k) \end{bmatrix}, \quad (15)$$

$$h(\mathbf{x}_k, u_k) = g[\text{SoC}(k)] - V_1(k) - V_2(k) - R_0 I(k). \quad (16)$$

3 Experiment and calculation method

To extract parameters of the LiFePO₄ polymer battery cell at very high hydrostatic pressure and low temperature, a series of tests were conducted on the cell under specific environmental conditions. The specifications of the cell are listed in Table 1.

3.1 Experimental setup

The experimental setup (Fig. 2a) comprises a battery test device (Neware BTS 4000), incubators (BLH-100), an auxiliary data acquisition system, an upper computer, a pressure barrel with a pressure gauge, and a pressurized pump. Photographs of all the equipment are shown in Fig. 2b. The incubator provides the ambient temperature from 3 to 20 °C and simulates the low temperature at the bottom of the sea. The pressure barrel, able to stand over 100 MPa, was used to simulate the pressure at 10 000 m in deep sea. Unfortunately, due to the limitations of our facilities, environments with both low temperature and high pressure could not be simulated.

Table 1 Specifications of LiFePO₄ polymer battery cell

Item	Description
Model	DJ-3.2 V, 3 Ah
Anode material	LiFePO ₄
Nominal voltage (V)	3.2
Voltage limit (V)	2.50–3.65
Nominal capacity (Ah)	3
Mass (g)	92
Dimensions (length×width×height, mm)	90×65×9.5
Cycle life (time)	≥1500
Operation temperature (°C)	−20–70

3.2 Experimental process

The experiment process is illustrated in Fig. 3. We emptied the battery at normal atmosphere pressure to achieve a low energy level at the beginning of pressurization. A constant current (CC) was implemented in the cell both in charge and discharge at different rates under the high hydraulic pressure. As the pressure rises, once the terminal voltage of the cell becomes abnormal, which usually means a battery is undergoing physical decomposition, a decompression procedure would start up to end the test immediately. When the pressure reached 100 MPa, a long standing time was allowed to evaluate whether the cell could survive at such a high pressure.

For extracting the parameters of the battery cell, a series of tests were conducted, including an OCV test, the maximum capacity test, and the HPPC test (Belt, 2010) in three different environments: 20 °C/0.1 MPa, 20 °C/100 MPa, and 3 °C/0.1 MPa.

The results of the maximum available capacity test were presented in Table 2. The OCV test provides the relationship between the OCV and SoC, and the relationship of OCV-SoC at 20 °C/0.1 MPa is fitted with a nonlinear function (Eq. (6)). Before each OCV test, the cell was fully charged and rested for 3 h to reach the equilibrium state. The cell was firstly discharged by 0.5 °C constant current for 300 s, and rested for 1 h. Once the terminal voltage reached the

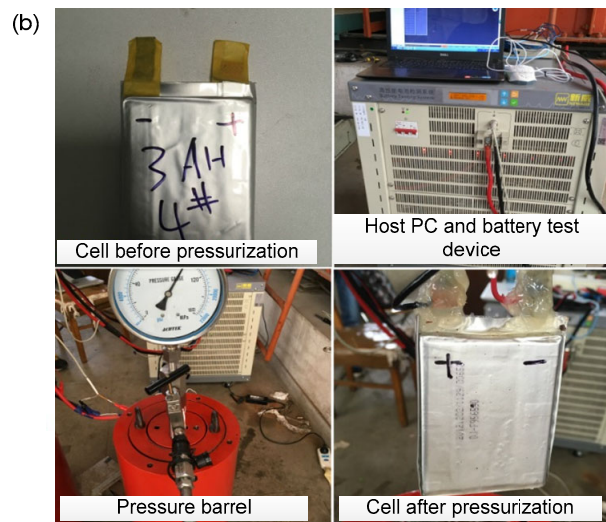
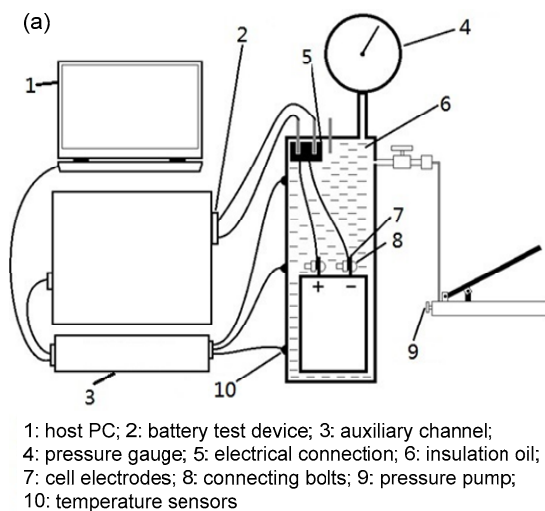


Fig. 2 A schematic of the experimental setup (a); Photographs of the battery test bench (b)

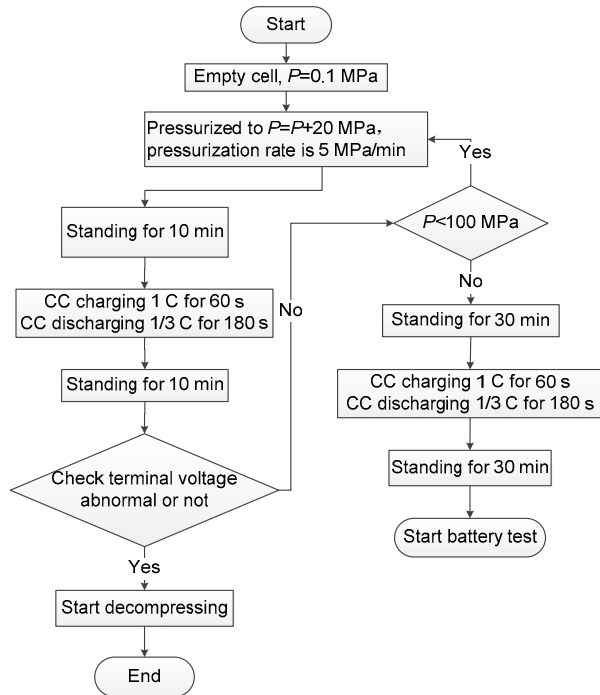


Fig. 3 Flow chart of the experimental process

Table 2 The maximum available capacity of the cell in different environments

Environmental condition	Maximum available capacity (Ah)
20 °C/0.1 MPa	2.80
20 °C/100 MPa	2.60
3 °C/0.1 MPa	2.54
Decompressing to 20 °C/0.1 MPa	2.80

target voltage during the discharge, the discharge rate was changed to 0.01 °C for 300 s and the cell was rested for 600 s. As soon as the terminal voltage reached the target voltage during the discharge, the test ended. The last point voltage of the rest stage was recorded as the OCV. The OCV-SoC curves were presented in Fig. 4a. Fig. 4b shows the differences in OCV of three curves from SoC of 10%–95%. Compared to the OCV-SoC curve at 20 °C/0.1 MPa, the curve for 3 °C/0.1 MPa is lower by 12 mV on average and the curve for 20 °C/100 MPa is higher by 15 mV on average. Differences in OCV would interfere with SoC estimation. If the differences are ignored during calculation, on average the estimation error would be 15% at 3 °C/0.1 MPa and 20% at 20 °C/100 MPa. Thus, compensation for temperature and pressure is essential for the ECM and SoC estimation algorithm. In this study, compensation was achieved through re-fitting the OCV-SoC curve in different environmental conditions. The compensated OCV-SoC functions at 3 °C/0.1 MPa and 20 °C/100 MPa are given by Eqs. (17) and (18), respectively:

$$g(\text{SoC}) = 2.905 + 0.664\text{SoC} - 0.4003\text{SoC}^2 - 0.06278 / \text{SoC} - 0.3124\ln(\text{SoC}) - 0.1199\ln(1.1 - \text{SoC}), \quad (17)$$

$$g(\text{SoC}) = -0.03536\text{SoC}^6 + 0.1589\text{SoC}^5 - 0.2131\text{SoC}^4 + 0.08122\text{SoC}^3 - 0.001271\text{SoC}^2 + 0.04292\text{SoC} + 3.271. \quad (18)$$

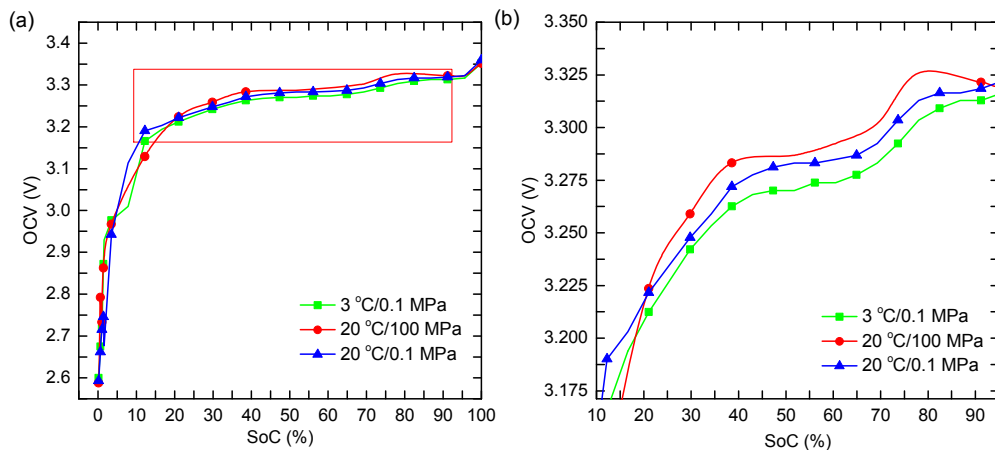


Fig. 4 OCV-SoC relationship in three environments (a); Partial enlarged detail from Fig. 4a (b)

The HPPC test was used to extract the cell parameters R_i ($i=0, 1, 2$) and C_i ($i=1, 2$). The test was conducted with SoC from 10% to 90%, at 10% intervals. The voltage and current profiles of the HPPC test are presented in Figs. 5a and 5b, respectively. The instantaneous voltage changes when the discharge current pulse was used to calculate the parameter R_0 , while the remaining dynamic part was used to calculate the parameters R_i ($i=1, 2$) and C_i ($i=1, 2$). Parameters were calculated by the method of Schweighofer et al. (2003) and are plotted in Fig. 6. The variations of ECM parameters are quite distinct. Compared with the parameter values of the ECM at 20 °C/0.1 MPa, the average increases of R_0 , R_1 , and R_2 are 3.24 m Ω , 0.3 m Ω , and 1.8 m Ω , respectively. The average decrease of C_1 is 48 F, and the average decrease of C_2 is 72 F at 20 °C/100 MPa. Similarly, the average increases of R_0 , R_1 , and R_2 are 11.4 m Ω , 2.7 m Ω , and 8 m Ω , respectively, and the average decreases of C_1 and C_2 are 298 F and 340 F, respectively, at 3 °C/0.1 MPa compared to the parameter values of the ECM at 20 °C/0.1 MPa.

4 SoC estimation based on UKF algorithm

Since the ECM parameters change distinctly with pressure and temperature, we used the UKF algorithm to evaluate the effectiveness of the estimation of the SoC of the battery.

4.1 UKF algorithm

The problem of battery SoC estimation can be converted to the solution of an inner hidden state from

a strong time-varying nonlinear system (He et al., 2013). The extended Kalman filter (EKF) has been proposed to solve nonlinear problems and has achieved remarkable success (Hu et al., 2011; Dong et al., 2016; Meng et al., 2016; Paschero et al., 2016). However, EKF considers only a first-order Taylor expansion to approximate a nonlinear system. As a result, it will bring non-negligible error. Thus, as an improvement of EKF, the UKF algorithm has been proposed which can approximate to the third-order Taylor expansion. It uses classical statistical methods based on unscented transform (UT) linearized solutions for nonlinear systems. It is a more accessible approach for nonlinear systems (Wan and van der Merwe, 2000). Applications of the UKF algorithm to SoC estimation can be found in (Sun et al., 2011; He et al., 2013; He et al., 2016). The UT includes the following procedures:

(1) Generate sigma points

A set of sigma points can be generated from Eq. (19):

$$\chi_i = \begin{cases} \bar{x} + (\sqrt{(n+\kappa)P_x})_i, & i = 1, 2, \dots, n, \\ \bar{x} - (\sqrt{(n+\kappa)P_x})_i, & i = n+1, n+2, \dots, 2n, \\ \bar{x}, & i = 0, \end{cases} \quad (19)$$

where \bar{x} and P_x are the mean value and variance of the state vector x (n dimensions), respectively, κ is the scaling parameter, and sampling points $\{\chi_i\}$ can approximate the Gaussian distribution of state x .

(b) Nonlinear transformation of sigma points

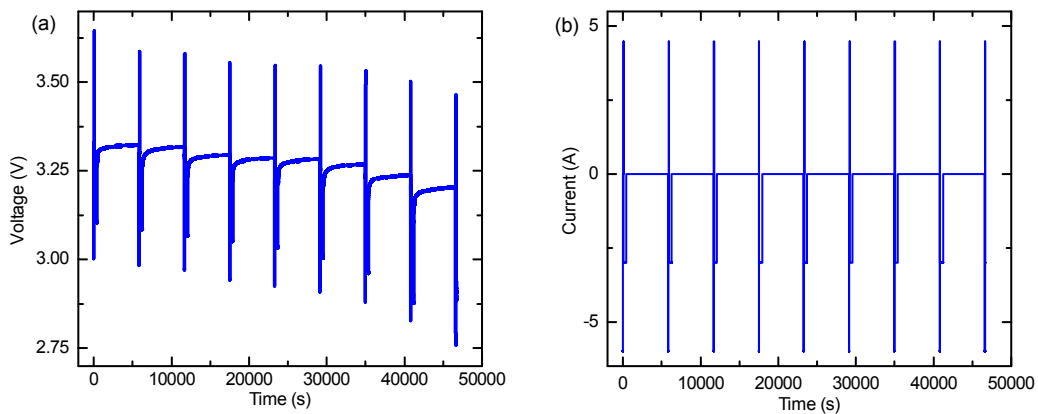


Fig. 5 HPPC test: (a) voltage profile; (b) current profile

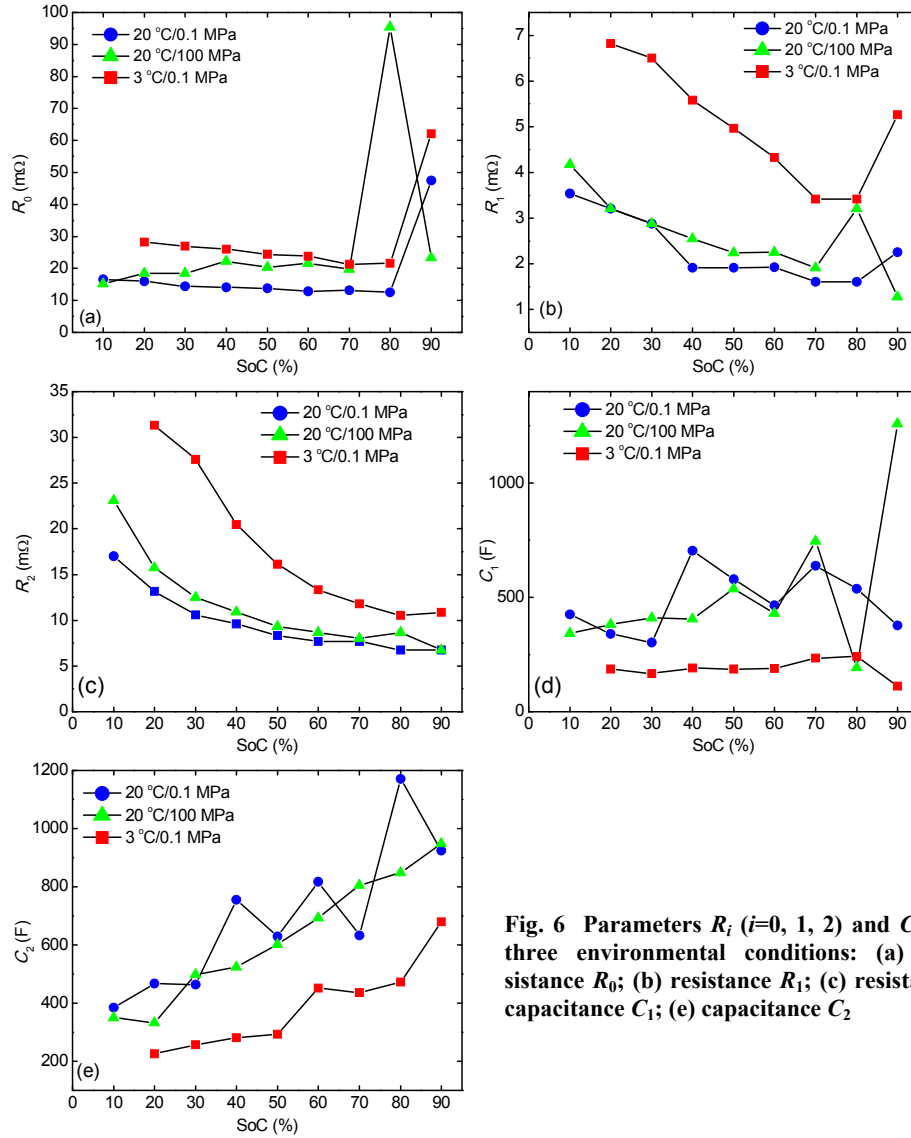


Fig. 6 Parameters R_i ($i=0, 1, 2$) and C_i ($i=1, 2$) in three environmental conditions: (a) ohmic resistance R_0 ; (b) resistance R_1 ; (c) resistance R_2 ; (d) capacitance C_1 ; (e) capacitance C_2

A set of new sigma points can be obtained through nonlinear transformation of $\{\chi_i\}$:

$$Y_i = f(\chi_i), \quad i = 0, 1, \dots, 2n. \quad (20)$$

The new set of points $\{Y_i\}$ can approximate the Gaussian distribution of $y=f(x)$.

(c) Calculate mean value and variance of y

The mean value and variance of y can be obtained from the set of sigma points $\{Y_i\}$ by a weighted approach:

$$\bar{y} \approx \sum_{i=0}^{2n} W_i^{(m)} Y_i, \quad (21)$$

$$P_y \approx \sum_{i=0}^{2n} W_i^{(c)} (Y_i - \bar{y})(Y_i - \bar{y})^T, \quad (22)$$

where $W_i^{(m)}$ and $W_i^{(c)}$ are the mean value and variance of y , respectively, which can be calculated from:

$$W_0^{(m)} = \kappa / (n + \kappa), \quad (23)$$

$$W_0^{(c)} = \kappa / (n + \kappa) + (1 - \alpha^2 + \beta), \quad (24)$$

$$W_i^{(m)} = W_i^{(c)} = \kappa / [2(n + \kappa)], \quad i = 1, 2, \dots, 2n, \quad (25)$$

where $\kappa = \alpha^2(n + \lambda) - n$. Parameters α , λ , and β are defined as: α is usually set to be a small real number, $e^{-4} < \alpha < 1$; λ is usually set to be 3 or $3 - n$; β is the

parameter used to adjust state distribution. For a Gaussian distribution, the optimal value of β is 2.

The details of the UKF algorithm in SoC estimation are summarized in Algorithm 1. To evaluate the effect of changing parameters on SoC estimation, a dynamic stress test (DST) cycle was implemented to simulate the real charge and discharge conditions of the battery. The current and terminal voltage profiles of the DST cycle are plotted in Figs. 7a and 7b, respectively.

4.2 SoC estimation results

To simplify the calculation, the mean values of the ECM parameters in the three environmental conditions were used as calibration values for the ECM (Table 3). The robustness of the UKF algorithm was proved by Sun et al. (2011) using an inaccurate initial state value. Therefore, we omit the analysis of algorithm robustness in this study.

Assuming the initial SoC value used for the UKF was not equal to the real initial SoC value, we initialized the SoC value $\hat{S}_0 = 80\%$ and set the DST cycle to start with SoC $S_0 = 100\%$. The initial parameters of the UKF algorithm are expressed as in

Table 3 Mean values of ECM parameters at 20 °C/0.1 MPa, 20 °C/100 MPa, and 3 °C/0.1 MPa

Environmental condition	R_0 (m Ω)	R_1 (m Ω)	R_2 (m Ω)	C_1 (F)	C_2 (F)
20 °C/0.1 MPa	17.90	2.3	9.7	486	694
20 °C/100 MPa	38.14	2.6	11.5	523	622
3 °C/0.1 MPa	29.30	5.0	17.7	188	354

Eq. (26). The variances of process noise and measurement noise are expressed as in Eq. (27). The SoC estimation results are plotted in Figs. 8a–8f.

Algorithm 1: UKF algorithm

1. Initialization

At time $k=0$, set $\hat{x} = E[x_0]$, $P_0 = E[(x_0 - \bar{x}_0)(x_0 - \bar{x}_0)^T]$.

2. State estimation for time step $k=1, 2, \dots, N$

(1) Calculate the sigma points

$$\begin{aligned}\chi_{k-1}^0 &= \hat{x}_{k-1}, \\ \chi_{k-1}^i &= \hat{x}_{k-1} + (\sqrt{(n+\kappa)P_{k-1}})_i, \quad i=1, 2, \dots, n, \\ \chi_{k-1}^i &= \hat{x}_{k-1} - (\sqrt{(n+\kappa)P_{k-1}})_i, \quad i=n+1, n+2, \dots, 2n.\end{aligned}$$

(2) Calculate the weight

$$\begin{aligned}W_0^{(m)} &= \kappa / (n + \kappa), \\ W_0^{(c)} &= \kappa / (n + \kappa) + (1 - \alpha^2 + \beta), \\ W_i^{(m)} &= W_i^{(c)} = \kappa / [2(n + \kappa)], \quad i=1, 2, \dots, 2n.\end{aligned}$$

(3) Update state vector

$$\begin{aligned}\chi_{k|k-1}^i &= f(\chi_{k-1}^i), \\ \hat{x}_k^- &= \sum_{i=0}^{2n} W_i^{(m)} \chi_{k|k-1}^i.\end{aligned}$$

(4) Update error and variance

$$P_{x,k}^- = \sum_{i=0}^{2n} W_i^{(c)} [\chi_{k|k-1}^i - \hat{x}_k^-][\chi_{k|k-1}^i - \hat{x}_k^-]^T + Q_k.$$

(5) Update output

$$\begin{aligned}\gamma_{k|k-1}^i &= h(\chi_{k|k-1}^i), \\ \hat{y}_k^- &= \sum_{i=0}^{2n} W_i^{(m)} \gamma_{k|k-1}^i.\end{aligned}$$

3. Measurement update

$$\begin{aligned}P_{y,k} &= \sum_{i=0}^{2n} W_i^{(c)} [\gamma_{k|k-1}^i - \hat{y}_k^-][\gamma_{k|k-1}^i - \hat{y}_k^-]^T + R_k, \\ P_{xy,k} &= \sum_{i=0}^{2n} W_i^{(c)} [\gamma_{k|k-1}^i - \hat{y}_k^-][\chi_{k|k-1}^i - \hat{x}_k^-]^T, \\ K &= P_{xy,k} P_{y,k}^{-1}, \\ \hat{x}_k &= \hat{x}_k^- + K(y_k - \hat{y}_k^-), \\ P_{x,k} &= P_{x,k}^- - K P_{y,k} K^T.\end{aligned}$$

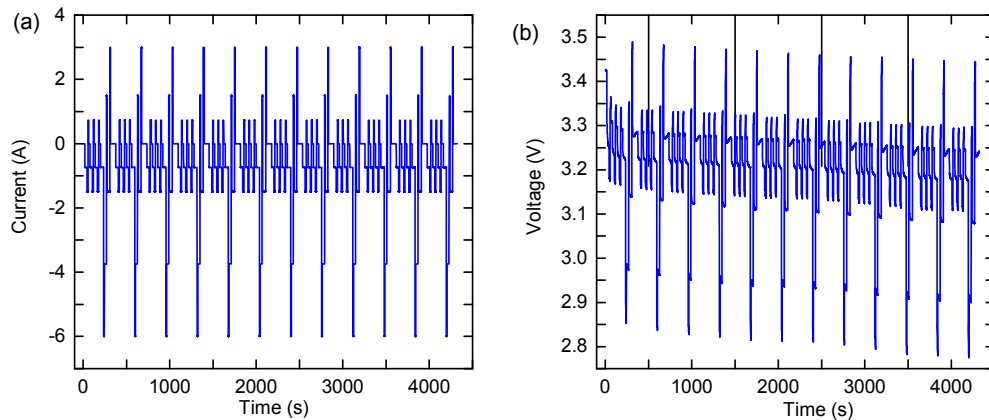


Fig. 7 DST cycle: (a) current profile; (b) voltage profile

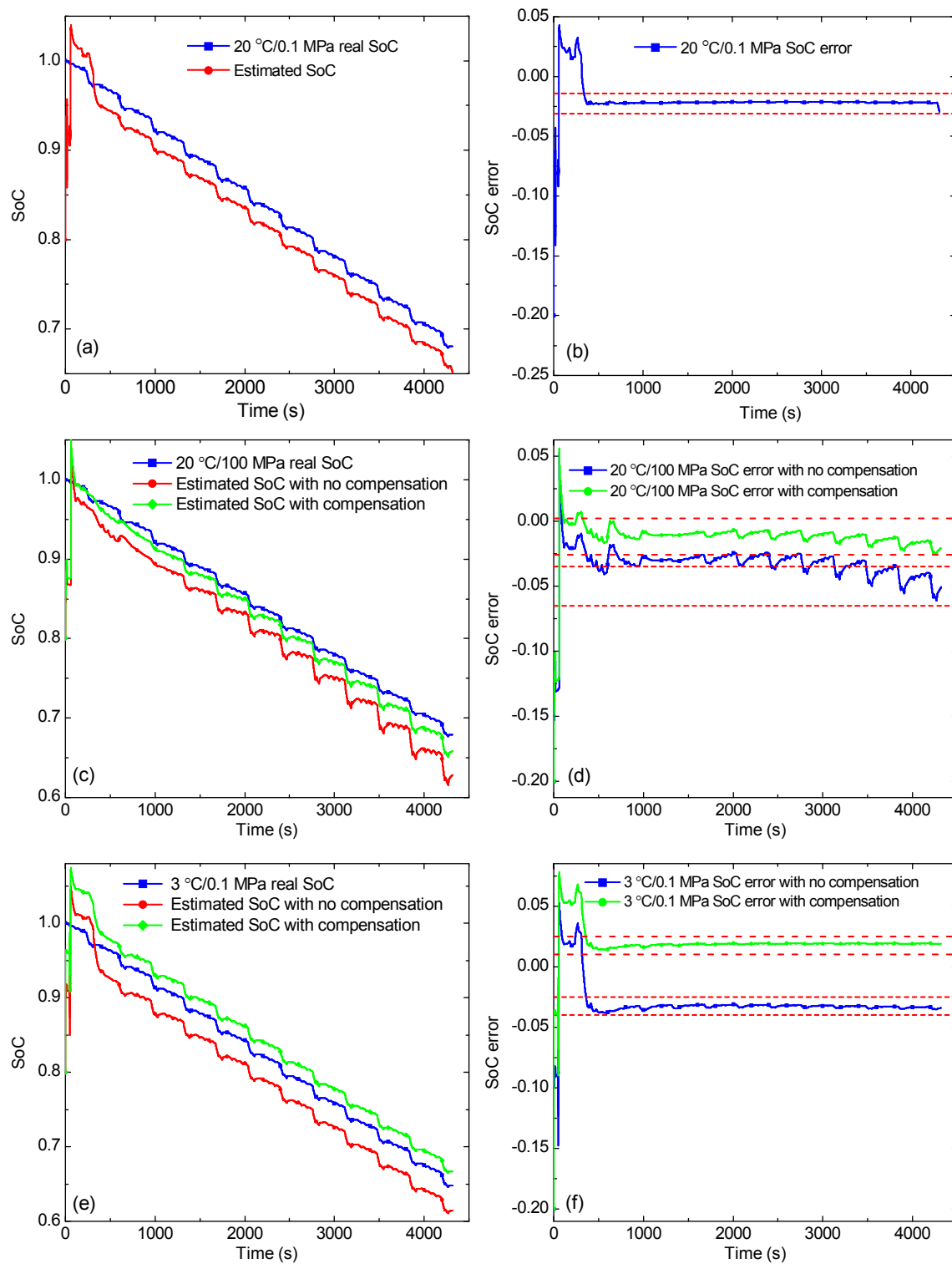


Fig. 8 SoC estimation results in different environments: (a) estimated value versus real value at 20 °C/0.1 MPa, (c) estimated value versus real value at 20 °C/100 MPa, (e) estimated value versus real value at 3 °C/0.1 MPa; (b) SoC estimation error at 20 °C/0.1 MPa, (d) SoC estimation error at 20 °C/100 MPa; (f) SoC estimation error at 3 °C/0.1 MPa

$$\begin{cases} \alpha=1, \\ \beta=2, \\ S_0=0.8, \\ \lambda=0, \\ V_{1(0)}=0, \\ V_{2(0)}=0, \end{cases} \quad (26)$$

$$\begin{cases} \mathbf{Q} = \begin{bmatrix} 0 & 0 & 0 \\ 0 & 0.00001^2 & 0 \\ 0 & 0 & 0.00001^2 \end{bmatrix}, \\ \mathbf{R} = [0.004^2]. \end{cases} \quad (27)$$

The algorithm can quickly converge to the real SoC values, and the absolute estimation errors are within 4%. The absolute mean SoC estimation error at 20 °C/0.1 MPa is 1.98%. The absolute mean estimation error increases to 3.32% at 20 °C/100 MPa and to 3.02% at 3 °C/0.1 MPa. The effect of hydrostatic pressure and low temperature on the estimation accuracy is obvious.

To alleviate the effect of high pressure and low temperature on UKF based SoC estimation, a kind of OCV-SoC compensation was proposed in this study, as shown in Eqs. (17) and (18), respectively. The results of SoC estimation with or without compensation versus real values in different environments are shown in Figs. 8c–8f. Compared to no compensation, the mean SoC estimation accuracy improved remarkably after compensation. The absolute mean estimation errors are 1.23% at 20 °C/100 MPa and 2.01% at 3 °C/0.1 MPa.

5 Conclusions

This paper reports the testing of a LiFePO₄ polymer battery cell operating at high pressure (100 MPa) and low temperature (3 °C). During the test, the battery cell was housed in a 100 MPa oil-filled pressure barrel to simulate the real working conditions of the battery pack in an ARV at 10000 m under the sea. The results show that a LiFePO₄ battery cell could survive in the 100 MPa environment without external physical or electrical failure.

The results of experiments and calculations comparing three different environments, 20 °C/0.1 MPa, 20 °C/100 MPa, and 3 °C/0.1 MPa, show that battery resistance increases and capacitance drops as ambient pressure increases and ambient temperature decreases.

In the simulated 10000 m deep sea environment, the effectiveness of a UKF-based estimation of the SoC of a lithium polymer battery was evaluated. The effect of high hydrostatic pressure and low temperature on estimation accuracy is obvious. The absolute mean estimation error increases to 3.32% at 20 °C/100 MPa and to 3.02% at 3 °C/0.1 MPa.

To alleviate the effect of high pressure and low temperature on UKF based SoC estimation, the functions OCV versus OCV-SoC at 100 MPa hydrostatic pressure and low temperature were compensated. The results show that SoC estimation accuracy is improved remarkably, with mean estimation errors reduced to 1.23% at 20 °C/100 MPa and 2.01% at 3 °C/0.1 MPa.

Acknowledgements

We would like to thank Shanghai Jiao Tong University Underwater Engineering Institute Co., Ltd., China for providing the pressure facilities and operating instructions.

References

- Belt JR, 2010. Battery Test Manual for Plug-in Hybrid Electric Vehicles. INL/EXT-07-12536, Idaho National Laboratory (INL), Idaho Falls, Idaho, USA.
- Dong GZ, Wei JW, Zhang CB, et al., 2016. Online state of charge estimation and open circuit voltage hysteresis modeling of LiFePO₄ battery using invariant imbedding method. *Applied Energy*, 162:163-171. <https://doi.org/10.1016/j.apenergy.2015.10.092>
- Griffiths G, Jamieson J, Mitchell S, et al., 2004. Energy storage for long endurance AUVs. *Proceedings of Advances in Technology for Underwater Vehicles*, p.8-16.
- Hasvold Ø, Størkersen N, 2001. Electrochemical power sources for unmanned underwater vehicles used in deep sea survey operations. *Journal of Power Sources*, 96(1): 252-258. [https://doi.org/10.1016/S0378-7753\(00\)00685-6](https://doi.org/10.1016/S0378-7753(00)00685-6)
- Hasvold Ø, Johansen KH, 2002. The alkaline aluminium hydrogen peroxide semi-fuel cell for the HUGIN 3000 autonomous underwater vehicle. *Proceedings of the 2002*

- Workshop on Autonomous Underwater Vehicles, p.89-94.
<https://doi.org/10.1109/AUV.2002.1177209>
- Hasvold Ø, Johansen KH, Mollestad O, et al., 1999. The alkaline aluminium/hydrogen peroxide power source in the Hugin II unmanned underwater vehicle. *Journal of Power Sources*, 80(1-2):254-260.
[https://doi.org/10.1016/S0378-7753\(98\)00266-3](https://doi.org/10.1016/S0378-7753(98)00266-3)
- Hasvold Ø, Lian T, Haakaas E, et al., 2004. CLIPPER: a long-range, autonomous underwater vehicle using magnesium fuel and oxygen from the sea. *Journal of Power Sources*, 136(2):232-239.
<https://doi.org/10.1016/j.jpowsour.2004.03.023>
- Hasvold Ø, Størkersen NJ, Forseth S, et al., 2006. Power sources for autonomous underwater vehicles. *Journal of Power Sources*, 162(2):935-942.
<https://doi.org/10.1016/j.jpowsour.2005.07.021>
- He HW, Qin HZ, Sun XK, et al., 2013. Comparison study on the battery SoC estimation with EKF and UKF algorithms. *Energies*, 6(10):5088-5100.
<https://doi.org/10.3390/en6105088>
- He HW, Xiong R, Peng JK, 2016. Real-time estimation of battery state-of-charge with unscented Kalman filter and RTOS μ COS-II platform. *Applied Energy*, 162:1410-1418.
<https://doi.org/10.1016/j.apenergy.2015.01.120>
- Hu XS, Sun FC, Cheng XM, 2011. Recursive calibration for a lithium iron phosphate battery for electric vehicles using extended Kalman filtering. *Journal of Zhejiang University-SCIENCE A (Applied Physics & Engineering)*, 12(11):818-825.
<https://doi.org/10.1631/jzus.A1100141>
- Liu F, Wang YH, Wu ZL, et al., 2017. Motion analysis and trials of the deep sea hybrid underwater glider Petrel-II. *China Ocean Engineering*, 31(1):55-62.
<https://doi.org/10.1007/s13344-017-0007-4>
- Meng JH, Luo GZ, Gao F, 2016. Lithium polymer battery state-of-charge estimation based on adaptive unscented Kalman filter and support vector machine. *IEEE Transactions on Power Electronics*, 31(3):2226-2238.
<https://doi.org/10.1109/TPEL.2015.2439578>
- Paschero M, Storti GL, Rizzi A, et al., 2016. A novel mechanical analogy-based battery model for SoC estimation using a multicell EKF. *IEEE Transactions on Sustainable Energy*, 7(4):1695-1702.
<https://doi.org/10.1109/TSSTE.2016.2574755>
- Rutherford K, Doerffel D, 2005. Performance of lithium-polymer cells at high hydrostatic pressure. *Proceedings of Symposium on Unmanned Untethered Submersible Technology*, p.1-12.
- Schweighofer B, Raab KM, Brasseur G, 2003. Modeling of high power automotive batteries by the use of an automated test system. *IEEE Transactions on Instrumentation and Measurement*, 52(4):1087-1091.
<https://doi.org/10.1109/TIM.2003.814827>
- Sidhu A, Izadian A, Anwar S, 2015. Adaptive nonlinear model-based fault diagnosis of Li-ion batteries. *IEEE Transactions on Industrial Electronics*, 62(2):1002-1011.
<https://doi.org/10.1109/TIE.2014.2336599>
- Stevenson P, Graham D, 2003. Advanced materials and their influence on the structural design of AUVs. In: Griffiths G (Ed.), *The Technology and Applications of Autonomous Underwater Vehicles*. Taylor & Francis, Abingdon, UK, p.77-91.
- Sun FC, Hu XS, Zou Y, et al., 2011. Adaptive unscented Kalman filtering for state of charge estimation of a lithium-ion battery for electric vehicles. *Energy*, 36(5):3531-3540.
<https://doi.org/10.1016/j.energy.2011.03.059>
- Wan EA, van der Merwe R, 2000. The unscented Kalman filter for nonlinear estimation. *Proceedings of 2000 Adaptive Systems for Signal Processing, Communications, and Control Symposium*, p.153-158.
<https://doi.org/10.1109/ASSPCC.2000.882463>
- Wang XM, Shang JZ, Luo ZR, et al., 2012. Reviews of power systems and environmental energy conversion for unmanned underwater vehicles. *Renewable and Sustainable Energy Reviews*, 16(4):1958-1970.
<https://doi.org/10.1016/j.rser.2011.12.016>
- Zou CF, Manzie C, Nešić D, 2016. A framework for simplification of PDE-based lithium-ion battery models. *IEEE Transactions on Control Systems Technology*, 24(5):1594-1609.
<https://doi.org/10.1109/TCST.2015.2502899>

中文概要

题目：深海环境对于 FeLiPO_4 聚合物电池性能的影响

目的：通过对万米深海环境中的高压和低温环境的模拟，研究深海环境对水下潜行器中动力电池性能所产生的影响以及该影响对电池剩余电量 (SoC) 估计精度的影响。

创新点：1. 通过压力桶和恒温箱模拟万米深海高压低温环境；2. 通过实验计算环境对电池模型参数的影响；3. 利用 UPF 算法对电池 SoC 进行估计并根据环境影响情况对开路电压 (OCV) 和 SoC 的关系进行补偿。

方法：1. 建立等效电路模型，建立电池系统状态空间方程 (公式 (1) ~ (16))；2. 通过混合功率脉冲测试 (HPPC) 对处于模拟深海环境中的电池进行等效电路模型参数辨识 (图 6)；3. 通过对 OCV-SoC 关系进行补偿得到低温高压环境下电

池的 OCV-SoC 关系式 (公式 (17) 和 (18));
4. 利用无迹卡尔曼滤波算法对常温常压环境和低温高压环境中的电池 SoC 进行估计 (图 8)。

结 论: 1. FeLiPO_4 聚合物锂离子电池能够在深海环境中正常使用, 但深海环境的高压低温特性会对电池参数本身产生影响; 2. 由于电池参数受高压低温

特性的影响, SoC 的估计误差会变大; 3. 通过对 OCV-SoC 关系的补偿能够在一定程度上提高电池 SoC 的估计精度, 从而减小由于参数变化带来的估计误差。

关键词: 锂离子聚合物电池性能; 深海环境; 剩余电量估计; 自治; 自治遥控潜水器